High-Resolution Ghost Image and Ghost Diffraction Experiments with Thermal Light

F. Ferri, D. Magatti, A. Gatti, M. Bache, E. Brambilla, and L. A. Lugiato

INFM, Dipartimento di Fisica e Matematica, Università dell'Insubria, Via Valleggio 11, 22100 Como, Italy

(Received 2 September 2004; published 12 May 2005)

High-resolution ghost image and ghost diffraction experiments are performed by using a single classical source of pseudothermal speckle light divided by a beam splitter. Passing from the image to the diffraction result solely relies on changing the optical setup in the reference arm, while leaving the object arm untouched. The product of spatial resolutions of the ghost image and ghost diffraction experiments is shown to overcome a limit which seemed to be achievable only with entangled photons.

DOI: 10.1103/PhysRevLett.94.183602 PACS numbers: 42.50.Dv, 42.50.Ar

The ghost imaging protocol provides a flexible way of performing coherent imaging by using spatially incoherent light. It relies on the use of two spatially correlated beams, one of them illuminating an object, while the other passes a reference optical setup. Information about the object is obtained by correlating the spatial distributions of the two beams. Traditionally parametric down-conversion (PDC) is the source of the correlated beams. In the low-gain regime the information is extracted from coincidence counts of single pairs of entangled signal-idler photons [1–4], while in the high-gain regime several photon pairs form entangled beams and the information is contained in the signal-idler correlation of the intensity fluctuations [5–8]. Landmark experiments in the low-gain regime showed that using entangled photons both the object image (the *ghost image* experiment [1]) and the object diffraction pattern (the *ghost diffraction* experiments [2,3]) could be retrieved.

Recently, a very lively debate arose aiming to identify which aspects (if any) of ghost imaging truly require entanglement. The first interpretation of the experiments suggested that entanglement of photon pairs was essential to retrieve information from the correlations [4]. This claim was challenged both by theoretical arguments [5] and by experiments [9,10], which showed that virtually any single result of ghost imaging could be reproduced by using classical sources with the proper kind of spatial correlation. However, some of us showed that only quantum entanglement provides perfect correlations both in photon position (near field) and in momentum (far field) [5,11], and (erroneously) suggested that this is crucial if both the image and the diffraction pattern are to be retrieved from the same source, leaving the object arm untouched [5]. In the same spirit, Ref. [10] pointed out that classical fields are subject to an uncertainty relation involving the product of conditional variances in position and momentum. This uncertainty relation has been invoked in experimental demonstrations of the Einstein-Podolsky-Rosen (EPR) paradox using photon pairs produced by PDC [12,13]. However, the same uncertainty relation was proposed as a limit for the product of the near-field and far-field imaging resolutions of a given classical source [10], suggesting thus that in ghost imaging only entangled photons can achieve high spatial resolution *simultaneously* in the near and in the far fields [10,12].

This scenario seems quite in contrast with the analyses of [6], where some of us proposed a special source of classically correlated beams capable of emulating the behavior of entangled beams in all the relevant aspects of ghost imaging, including the resolution abilities, although with a lower visibility. In the proposed scheme, an intense beam with a thermal-like statistics is divided by a beam splitter, and the two outgoing beams have strong spatial correlations simultaneously in the near-field and far-field planes. Because of this, the scheme is able to retrieve with a good resolution both the object image and the diffraction pattern by using the same source and operating only on the reference arm. In this Letter we provide the first—to our knowledge—experimental evidence of these results [14]. We show that the product of the near- and far-field resolutions obtained using the classical source is better than the entangled case of [10,12] and that it largely overcomes the bound of [10]. Despite a visibility substantially lower than 100%, we efficiently retrieve imaging information. This definitively demonstrates that entanglement is not necessary for ghost imaging.

The experimental setup is sketched in Fig. 1. The pseudothermal source is provided by a slowly rotating ground glass placed in front of a scattering cell containing a highly turbid solution of 3 μm latex spheres. When this system is illuminated by a large collimated laser beam ($\lambda = 0.6328$ μm, diameter $D_0 \approx 10$ mm), the stochastic interference of the waves emerging from the source produces a time-dependent speckle pattern, characterized by a corre-

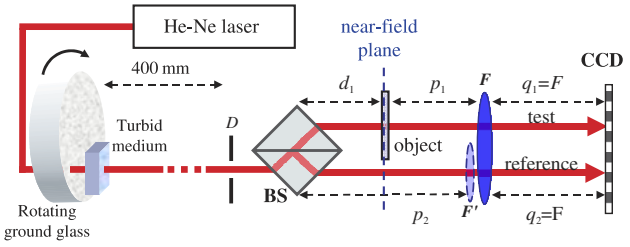

FIG. 1 (color online). Scheme of the experimental setup (see text for details).

lation time τ_{coh} on the order of 0.5 s. An angular portion of the speckle pattern is selected by a $D = 3$ mm diaphragm at a distance $z_0 = 400$ mm from the thermal source, allowing the formation of an almost collimated speckle beam. The beam is characterized by chaotic statistics [15] and by a large number ($\approx 10^4$) of speckles of size $\Delta x \approx \lambda z_0/D_0 \approx 25$ μm [15]. The beam is separated by the beam splitter (BS) into "twin" speckle beams, that exhibit a high (although classical) level of spatial correlation. The two beams (test beam "1" and reference beam "2") have slightly noncollinear propagation directions, and illuminate two nonoverlapping portions of the charged-coupled-device (CCD) camera. The data are acquired with an exposure time (1 ms) much shorter than τ_{coh}, allowing the recording of high-contrast speckle patterns. The frames are grabbed at a rate of 1 Hz, so that each data acquisition corresponds to uncorrelated speckle patterns. Notice that in our source the random motion of particles in the solution provides a truly random temporal statistics of light, while the ground glass ensures that there is no residual unscattered light.

We now demonstrate a high-resolution reconstruction of both the image (Fig. 2) and the diffraction pattern (Fig. 3) of the object by operating only on the optical setup of the reference arm and by using a single classical source. The optical setup of the object arm 1 is fixed. An object, consisting of a thin needle of 160 μm diameter inside a rectangular aperture 690 μm wide, is placed in this arm at a distance d_1 from the BS. A single lens of focal $F = 80$ mm is placed after the object, at a distance p_1 from the object and $q_1 = F$ from the CCD. Hence the CCD images the far-field plane with respect to the object. However, since the light is incoherent, the diffraction pattern of the object is not visible on the CCD, as shown in Fig. 3(a). We consider two different setups for the reference arm 2. In the first one, an additional lens of focal F' is inserted in arm 2 immediately before lens F. The equivalent focal F_2 of the two-lens system is smaller than its distance from the CCD $q_2 = F$, being $\frac{1}{F_2} \approx \frac{1}{F} + \frac{1}{F'}$. This allowed us to locate the position of the plane conjugate to the CCD plane, by temporarily inserting the object in arm 2 and determining the position that produced a well focused image on the CCD with laser illumination [Fig. 2(b)]. The object was then translated in the object arm. The distances in the reference arm approximately obey a thin lens equation of the form $1/(p_2 - d_1) + 1/q_2 \approx 1/F_2$, providing a demagnification factor $m \simeq 1.2$. The data of the intensity distribution of the reference arm are acquired, and each pixel is correlated with the total photon counts of arm 1, which corresponds to having a "bucket" detector there [1,4]. Averages performed over 5000 data acquisitions show a well-resolved image of the needle [Fig. 2(a)] that can be compared with the image obtained with laser illumination [Fig. 2(b)]. Figure 2(c) compares the corresponding horizontal sections, averaged over 500 pixels in the vertical direction. The spatial resolution shown by correlated imaging with incoherent light is comparable with that obtained via coherent illumination.

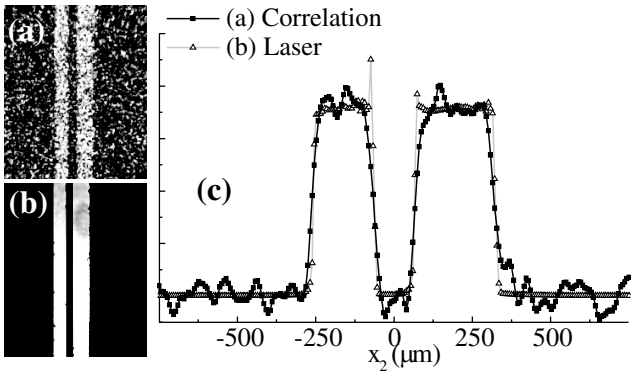

FIG. 2. Reconstruction of the object image. (a) Correlation of intensity fluctuations. (b) Image observed using laser light. (c) Averages of 500 horizontal data sections from (a) and (b).

In the second setup lens F' is simply removed from the scheme of Fig. 1, so that the CCD is in the focal plane of lens F also in arm 2. The spatial cross correlation of the intensities is calculated as a function of the displacement $\vec{x}_2 - \vec{x}_1$ between the pixel positions in the two arms, by making an additional average over pixel positions at each fixed $\vec{x}_2 - \vec{x}_1$ [7,8]. Thus, averages over only 500 independent frames are enough to show a sharp reproduction of the diffraction pattern of the object [Fig. 3(b)]. This is compa-

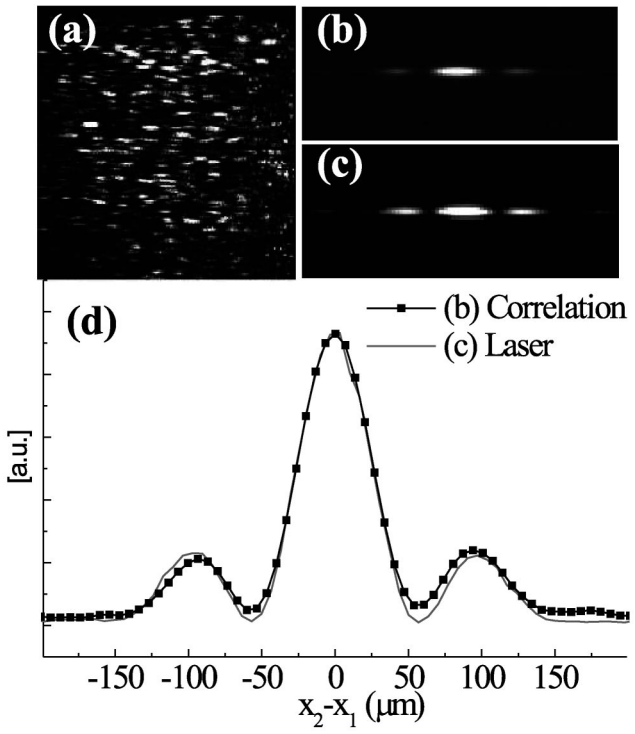

FIG. 3. Reconstruction of the diffraction pattern. (a) Single-shot intensity distribution in arm 1. (b) Intensity fluctuation correlation $G(\vec{x}_2 - \vec{x}_1)$. (c) Object diffraction pattern observed using laser light. (d) Horizontal cut of (b) and (c).

rable with the diffraction pattern obtained by laser illumination [Fig. 3(c)]. Horizontal sections of the two patterns display a very good agreement [Fig. 3(d)].

The theory behind the setup shown in Fig. 1 has been explained in detail in Ref. [6]. The speckle field is characterized by Gaussian field statistics [15], in which any correlation function of arbitrary order is expressed via the field correlation function

$$\Gamma(\vec{x}, \vec{x}') = \langle a^\dagger(\vec{x}) a(\vec{x}') \rangle, \tag{1}$$

where $a(\vec{x})$ is the boson annihilation operator of the speckle field. The object information is extracted by measuring the spatial correlation function of the intensities $\langle I_1(\vec{x}_1) I_2(\vec{x}_2) \rangle$, where $I_i(\vec{x}_i)$ is the number of photocounts over the CCD pixel located at $\vec{x}_i$ in the ith beam, and subtracting the background term $\langle I_1(\vec{x}_1) \rangle \langle I_2(\vec{x}_2) \rangle$, therefore obtaining the correlation of intensity fluctuations [6]

$$\begin{aligned} G(\vec{x}_1, \vec{x}_2) &= \langle I_1(\vec{x}_1) I_2(\vec{x}_2) \rangle - \langle I_1(\vec{x}_1) \rangle \langle I_2(\vec{x}_2) \rangle \\ &= |rt|^2 \left| \int d\vec{x}_1' d\vec{x}_2' h_1^*(\vec{x}_1, \vec{x}_1') h_2(\vec{x}_2, \vec{x}_2') \Gamma_n(\vec{x}_1', \vec{x}_2') \right|^2, \end{aligned} \tag{2}$$

where r and t are the reflection and transmission coefficients of the BS, $\Gamma_n(\vec{x}_1', \vec{x}_2')$ is the second order correlation function (1) of the speckle field at the object (near-field) plane, while h_1 and h_2 are the impulse response functions describing the optical paths of beams 1 and 2 from the object to the CCD plane [16]. The setup of arm 1 is kept fixed, and $h_1(\vec{x}_1, \vec{x}_1') \propto e^{-i\vec{x}_1 \cdot \vec{x}_1' k/F} T(\vec{x}_1')$, where $T(\vec{x})$ is the object transmission function and $k = 2\pi/\lambda$. For the ghost image setup used in Fig. 2, apart from inessential phase factors $h_2(\vec{x}_2, \vec{x}_2') = m\delta(m\vec{x}_2 + \vec{x}_2')$. Inserting this in Eq. (2):

$$G(\vec{x}_1, \vec{x}_2) \propto \left| \int d\vec{x}_1' \Gamma_n(\vec{x}_1', -m\vec{x}_2) T^*(\vec{x}_1') e^{i\vec{x}_1 \cdot \vec{x}_1' k/F} \right|^2 \tag{3}$$

$$\approx |T(-m\vec{x}_2)|^2 \left| \int d\vec{x}_1' \Gamma_n(\vec{x}_1', -m\vec{x}_2) e^{i\vec{x}_1 \cdot \vec{x}_1' k/F} \right|^2. \tag{4}$$

Equation (4) was derived under the assumption that the smallest scale over which the object changes is larger than the length over which $\Gamma_n(\vec{x} - \vec{x}')$ decays, which we refer to as the *near-field coherence length* Δx_n. In general, the result of a measurement of G in this setup is a convolution of the object transmission function with the near-field correlation function Γ_n, so that Δx_n sets the spatial resolution for the reconstruction of the image. Note that what we observe in Fig. 2(a) is $\int d\vec{x}_1 G(\vec{x}_1, \vec{x}_2)$, because of the bucket detection scheme in arm 1, which makes the imaging incoherent [4,8]. In the ghost diffraction experiment the detection plane of beam 2 is the focal plane of lens F. Hence, $h_2(\vec{x}_2, \vec{x}_2') \propto e^{-i\vec{x}_2 \cdot \vec{x}_2' k/F}$. From Eq. (2), we obtain

$$G(\vec{x}_1, \vec{x}_2) \propto \left| \int d\vec{\xi} \Gamma_f(\vec{\xi}, \vec{x}_2) \tilde{T}^*[(\vec{x}_1 - \vec{\xi})k/F] \right|^2 \tag{5}$$

$$\approx |\tilde{T}[(\vec{x}_1 - \vec{x}_2)k/F]|^2 \left| \int d\vec{\xi} \Gamma_f(\vec{\xi}, \vec{x}_2) \right|^2, \tag{6}$$

where $\tilde{T}(\vec{q}) = \int \frac{d\vec{x}}{2\pi} e^{-i\vec{q} \cdot \vec{x}} T(\vec{x})$. $\Gamma_f(\vec{x}, \vec{x}')$ is the field correlation (1) observed in the focal plane of lens F; its correlation length Δx_f (the *far-field coherence length*) sets the spatial resolution limit for reconstructing the diffraction pattern.

Relevant to the resolution of the ghost image and ghost diffraction schemes are hence the spatial coherence properties of the speckle beam in the near and far fields. These can be investigated by measuring the fourth-order correlation functions, in the absence of the object. The autocorrelation function of the reference beam $\langle I_2(\vec{x}) I_2(\vec{x}') \rangle$ was first measured in the setup with lens F' inserted, so that the reference beam recorded by the CCD is the (demagnified) image of the near field. This is plotted in Fig. 4 (squares) as a function of $|\vec{x} - \vec{x}'|$. Neglecting the shot noise contribution at $\vec{x} = \vec{x}'$, and using the Siegert formula for Gaussian statistics, we get

$$\langle I_2(\vec{x}) I_2(\vec{x}') \rangle = \langle I_2(\vec{x}) \rangle \langle I_2(\vec{x}') \rangle + |r|^4 |\Gamma_n(m\vec{x}, m\vec{x}')|^2. \tag{7}$$

The baseline in Fig. 4 corresponds to the product of the mean intensities, while the narrow peak around $\vec{x} = \vec{x}'$ is the second term on the right-hand side of (7). A Gaussian fit of this peak gave a variance $\sigma_n = (14.3 \pm 0.2)$ μm, implying a coherence length in the near-field plane $\Delta x_n \approx 2m\sigma_n = (34.3 \pm 0.6)$ μm. The triangles in Fig. 4 plot the intensity correlation function in the far-field plane, obtained by measuring the autocorrelation function of beam 1 in the focal plane of lens F. The narrow peak in this plot is $\propto |\Gamma_f(\vec{x}, \vec{x}')|^2$. A Gaussian fit gave $\sigma_f = (7.8 \pm 0.3)$ μm, from which we infer a far-field coherence length $\Delta x_f \approx 2\sigma_f = (15.6 \pm 0.6)$ μm. This in turn corresponds to a spread in transverse wave vectors $\Delta q = \frac{2\pi}{\lambda F} \Delta x_f = (1.94 \pm 0.07) \times 10^{-3}$ μm^{-1}.

Reference [10] identified the conditional variance with resolution, and argued that the product of the near-field and far-field resolutions for a classical system cannot be lower than unity. We find for our classical beams

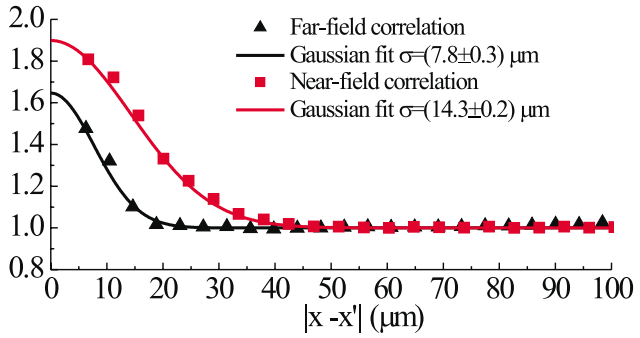

FIG. 4 (color online). Normalized fourth-order autocorrelation function in the near-field and far-field planes. The full lines are Gaussian fits of the correlation peaks.

$$\Delta x_n \Delta q = 0.066 \pm 0.003. \quad (8)$$

This result clearly violates the proposed limit despite originating from nonentangled beams, and it is roughly 4 times smaller than the results reported in Refs. [10,12], where entangled photons were used. Notice that Eq. (8) is not violating any EPR bound. In fact, in any plane, the probability of detecting a photon at position $\vec{x}_2$ in beam 2 conditioned to the detection of a photon at $\vec{x}_1$ in beam 1 is

$$P(\vec{x}_2|\vec{x}_1) \propto \langle I_2(\vec{x}_2) I_1(\vec{x}_1)\rangle / \langle I_1(\vec{x}_1)\rangle = \langle I_2(\vec{x}_2)\rangle + |rt|^2 |\Gamma(\vec{x}_1, \vec{x}_2)|^2 / \langle I_1(\vec{x}_1)\rangle. \quad (9)$$

The two terms in Eq. (9) have roughly the same height (see Fig. 4), but the first one, originating from the background, is much broader than the second, because the beam diameter is much larger than the coherence length. Hence, in good approximation the conditional variance in position is the beam spot size. The product of the variances in the near and far zones satisfy a Fourier relation in accordance with the bound derived in [10]. The crucial point is that the conditional variance and the resolution of ghost imaging do not coincide in general, since the resolution is determined by the coherence length of the *field* correlation function $\Gamma(\vec{x}, \vec{x}')$ [see Eqs. (3) and (5)]. They do coincide only in the special case where the background is negligible, as, e.g., in the coincidence count regime of PDC considered by [10,12]. Only in this case, which in principle corresponds to 100% visibility, the bound of [10] holds also for resolutions. In this respect, there is no formal contradiction between our results and the arguments of [10], where only *high-contrast* imaging was considered. In our experiment, where the visibility is limited to 50%, the product of the near and far-field resolutions is not bounded, because the coherence lengths (the speckle sizes) in the two planes are independent quantities. In the near field, the size of the speckles depends on the laser diameter D_0, and on the distance z from the source, $\Delta x_n \propto \lambda z / D_0$ [15]. As we checked, the diaphragm being close enough to the near field, its diameter D does not affect much Δx_n. D, instead, determines the speckle size in the far field, roughly given by $\Delta x_f \propto \lambda F / D$ [15]. Using the values of our setup, we find $\Delta x_n \approx 30$ μm and $\Delta x_f \approx 17$ μm, in good agreement with the values estimated from the correlation (Fig. 4). Two aspects of our experiment are crucial: (i) the presence in the near field of a large number of small speckles inside a broad beam, and (ii) a measurement time $\ll \tau_{\mathrm{coh}}$. This allows the formation by interference of a far-field speckle pattern, characterized by a small coherence length because $\Delta x_f \propto 1/D$. In this respect our source differs from the classical one used in [9,10], where each shot consists of a single narrow pulse and the product of resolutions is bounded by the pulse diffraction.

In conclusion, we have reported on high-resolution ghost image and ghost diffraction experiments by using a single source of classically correlated thermal light. The distributed imaging character is evident from the fact that the object information can be processed by acting only on the reference beam. The product of resolutions of the ghost image and the ghost diffraction schemes is well below the limit that was suggested to be achievable only with entangled beams, and could even be further improved by optimizing the scheme. This definitely proves the claim set forth in [6], that the only advantage of entanglement with respect to classical correlation lies in the better visibility of information. This implies a better signal-to-noise ratio, which is important in high sensitivity measurements or in quantum information schemes (where, e.g., the information needs to be hidden for a third party), but it does not give any practical advantage in processing information from a macroscopic classical object, as used here.

This work was supported by FET QUANTIM, COFIN of MIUR, INTAS 2001-2097, and the Carlsberg Foundation.

[1] T. B. Pittman, Y. H. Shih, D. V. Strekalov, and A. V. Sergienko, Phys. Rev. A **52**, R3429 (1995).
[2] D. V. Strekalov, A. V. Sergienko, D. N. Klyshko, and Y. H. Shih, Phys. Rev. Lett. **74**, 3600 (1995).
[3] P. H. Souto Ribeiro, S. Padua, J. C. Machado da Silva, and G. A. Barbosa, Phys. Rev. A **49**, 4176 (1994).
[4] A. F. Abouraddy, B. E. A. Saleh, A. V. Sergienko, and M. C. Teich, Phys. Rev. Lett. **87**, 123602 (2001); J. Opt. Soc. Am. B **19**, 1174 (2002).
[5] A. Gatti, E. Brambilla, and L. A. Lugiato, Phys. Rev. Lett. **90**, 133603 (2003).
[6] A. Gatti, E. Brambilla, M. Bache, and L. A. Lugiato, Phys. Rev. A **70**, 013802 (2004); Phys. Rev. Lett. **93**, 093602 (2004).
[7] M. Bache, E. Brambilla, A. Gatti, and L. A. Lugiato, Phys. Rev. A **70**, 023823 (2004).
[8] M. Bache, E. Brambilla, A. Gatti, and L. A. Lugiato, Opt. Express **12**, 6067 (2004).
[9] R. S. Bennink, S. J. Bentley, and R. W. Boyd, Phys. Rev. Lett. **89**, 113601 (2002).
[10] R. S. Bennink, S. J. Bentley, R. W. Boyd, and J. C. Howell, Phys. Rev. Lett. **92**, 033601 (2004).
[11] E. Brambilla, A. Gatti, M. Bache, and L. A. Lugiato, Phys. Rev. A **69**, 023802 (2004).
[12] M. D'Angelo, Y.-H. Kim, S. P. Kulik, and Y. Shih, Phys. Rev. Lett. **92**, 233601 (2004).
[13] J. C. Howell, R. S. Bennink, S. J. Bentley, and R. W. Boyd, Phys. Rev. Lett. **92**, 210403 (2004).
[14] A. Valencia, G. Scarcelli, M. D'Angelo, and Y. Shih, Phys. Rev. Lett. **94**, 063601 (2005), reports a ghost image experiment with thermal photons but does not consider the ghost diffraction and the resolution issues.
[15] J. W. Goodman, in *Laser Speckle and Related Phenomena*, Topics in Applied Physics Vol. 9, edited by D. Dainty (Springer, Berlin, 1975), p. 9.
[16] D. Magatti *et al.*, quant-ph/0408021.